Moment-Curvature Relationships in Reinforced Concrete

by

M.N. Nagendra Prasad

Thesis submitted to the Faculty of the
Virginia Polytechnic Institute and State University
in partial fulfillment of the requirements for the degree of
Master of Science
in
Civil Engineering

APPROVED

R.M. Barker, Chairman

S.M. Holzer

D.A. Garst

July 1993
Blacksburg Virginia

Moment-Curvature Relationships in Reinforced Concrete

by

M.N. Nagendra Prasad

Committee Chairman Dr. R.M. Barker

Civil Engineering

(ABSTRACT)

The purpose of this study is to investigate the effects of tension stiffening and softening of concrete in reinforced concrete beams and beam-columns. Analytical models of beams and beam-columns are prepared and the results compared to experimental results previsously conducted by Berwanger et al. (1960)

A layered model of the beams is developed and strains and stresses at various layers are computed. Moment-curvature relationships are then obtained from these. The stress-strain curves adopted are from El-Metwally and Chen (1989). The effects of tension stiffening and softening are included by adopting realistic stress-strain curves in both compression and tension.

Acknowledgments

I am greatly indebted to my advisor, Dr. R.M. Barker for his continued academic guidance and moral support. I would like to thank him for being so patient and understanding throughout my study here at Virginia Tech. I would also like to thank Dr. Holzer and Dr. Garst for serving in the committee and for their cooperation without which I would not have been able to schedule my examination at such a short notice.

I would like to thank my family and friends back home, without whose sacrifices and support this would not have been possible. I am grateful to all my friends here for their help and for making my stay in Blacksburg memorable.

Table of Contents

List of Figures

Chapter 1: Introduction

Reinforced concrete is by far one of the most commonly used construction materials. Because concrete is relatively weak and brittle in tension, concrete cracking as well as interactions between steel and concrete can cause highly nonlinear behavior. The flexural and axial rigidities of the members are functions of current state of strain and/or load in a nonlinear analysis of reinforced concrete frames. This, in general makes it very difficult to obtain a closed form solution for evaluating stiffnesses. A convenient way of expressing a measure of stiffness of a member is to obtain the moment-curvature relation. Hence a numerical method for determining moment-curvature relationships would be helpful in the nonlinear analysis of reinforced concrete frames.

1.1 Moment-Curvature Relationships

Moment-curvature relationships are given by Alwis (1990) as a trilinear model with three identification points (cracking, yielding and ultimate moment). Figure 1.1 shows this model. This model is relatively simple to formulate and convenient when

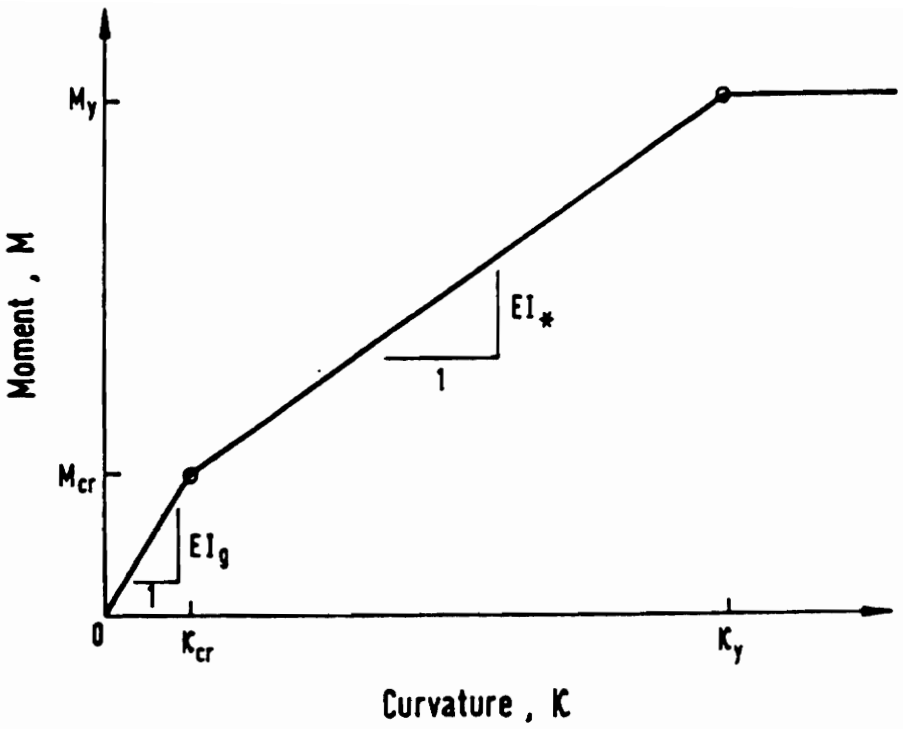

Figure 1.1. Trilinear moment-curvature model given by Alwis (1990)

applied for deflection analysis using numerical methods. However, the three identification points can be clearly defined only in the case of beams and are not readily available for beam-columns. A sudden change of slope or stiffness can introduce numerical difficulty.

1.2 Numerical Method by El-Metwally and Chen

A numerical method for the development of moment-curvature and axial force-axial strain has been developed by El-Metwally and Chen (1990). This method utilizes continuous stress-strain curves and avoids the sudden change in slope. They have compared the analytical results to the experimental results of Berwanger et al. (1960). Two series of beams have been tested by Berwanger. The first series consisted of two beams simply supported and the second series had six continuous beams. Shear reinforcement in the beams was varied. El-Metwally and Chen have made comparisons to both of Berwanger's series and have also looked at the effect of axial load on the moment-curvature relationships. These consist of parametric studies but they have not been compared to any experimental results.

1.2.1 Comparison of results obtained by El-Metwally and Chen with Berwanger's experimental data.

Figure 1.2 shows the analytic moment-curvature versus the experimental data for three beams tested by Berwanger. As is clear from the figure, the analytical results are not in complete agreement with the experimental data. The analytical predictions show a sudden change in stiffness after cracking. The results also do not show a smooth transition from an uncracked section to a fully cracked section.

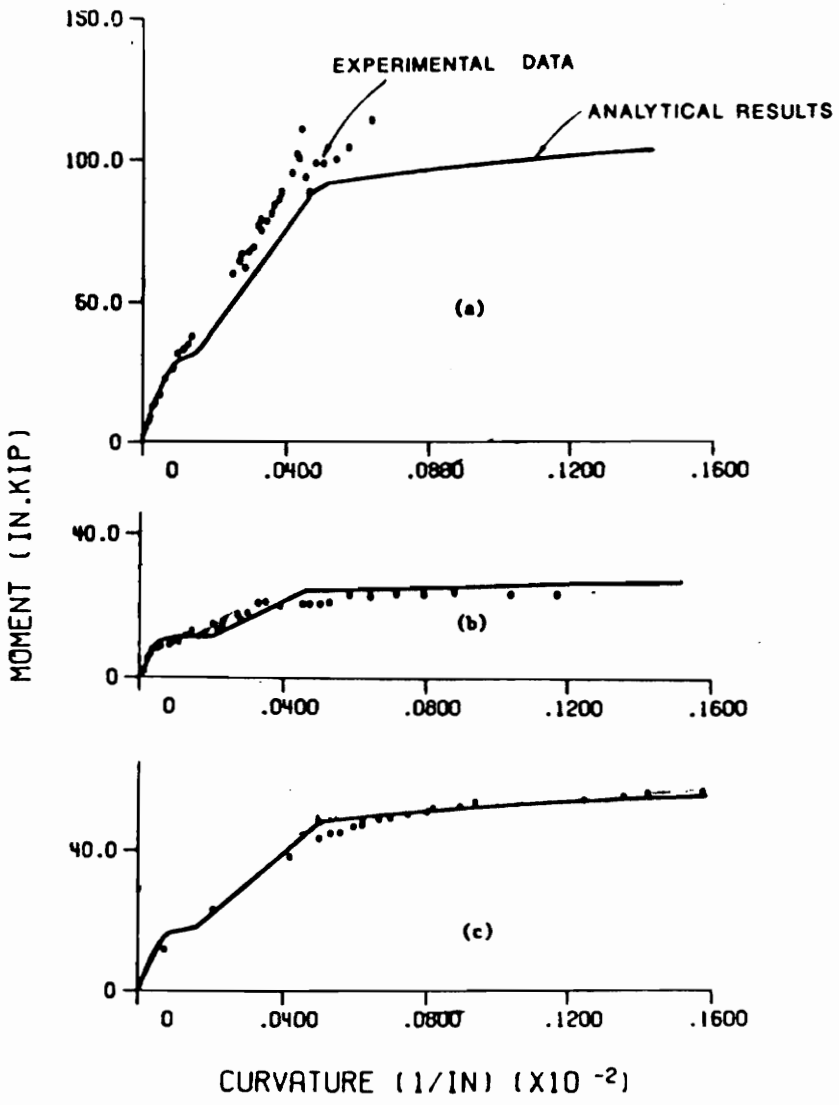

Figure 1.2. Analytic Moment Curvature relationship versus Experimental data.

1.2.2 Reasons for disparity between the experimental and analytical results

According to El-Metwally and Chen, the reason for the disparities could be due to the fact the method ignores the 'tension stiffening' effect described in Chapter 2. A similar view has been expressed by Alwis (1990). Gilbert and Warner (1978) state that the tension stiffening effect has a considerable influence on the overall bending stiffness and that it is significant in beams. Cosena et al. (1991) in their paper have also given importance to this effect.

Another conclusion reached by El-Metwally and Chen regarding the disparities is that it may be because the method does not include the softening effect of concrete in tension. This effect, which has been observed experimentally, does alter the load carrying capacity of the beam. Gajer and Dux (1988) emphasize the need to incorporate the tension and compression softening phenomena in numerical methods. Bazant et al. (1987) have expressed similar views. The discussion is expanded in Chapter 2.

1.2.3 Stress-Strain Relationships in Concrete

Fundamental to the development of more accurate moment-curvature relationships is the correct description of stress-strain behavior of concrete in compression and tension. Figure 1.3 shows the stress-strain curves adopted by El-Metwally and Chen in compression. Three strain points ε_{ce}, ε_{cs} and ε_{cf} have been defined. The stress-strain curve varies parabolically up to ε_{ce}. It is assumed to be at a constant stress f_c' between ε_{ce} and ε_{cs}, after which it decreases linearly having a value of $0.8f_c'$ at ε_{cf}. An attempt

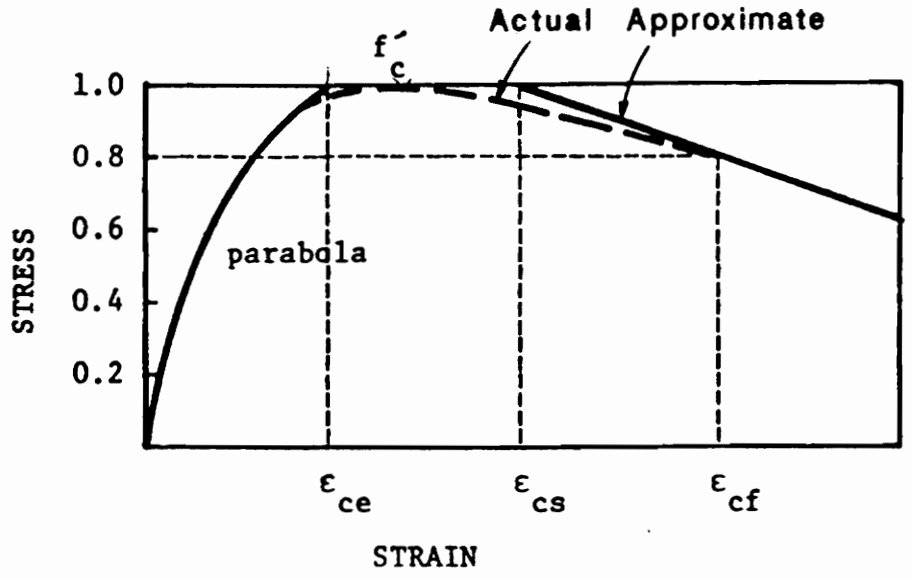

Figure 1.3. Stress-Strain Curve for Concrete in Compression adopted by El-Metwally and Chen

has been made to include the effects of bound concrete and stirrups. A factor 'q' has been included in the computation of f_c'. This factor depends on the area of bound concrete, area of transverse steel and spacing of transverse steel. A longitudinal spacing at which transverse reinforcement is not effective, is assumed as 10 inches. The strains ε_{cs} and ε_{cf} depend on q and ε_{ce} depends on E_c. The variations in the stress-strain curve due to changes in area of bound concrete and area of transverse reinforcement will be given in Chapter 3.

The stress-strain curve for concrete in tension adopted by El-Metwally and Chen (1990) is shown in Figure 1.4. This curve has been idealized and does not include the softening behavior. The stress is assumed to be zero after a strain ε_t is reached. Also the stress is taken as constant from $0.33\varepsilon_t$ to ε_t at a value f_t. From 0 to $0.33\varepsilon_t$ it is assumed to be linearly varying. The expressions for ε_t and f_t are defined in Figure 1.4.

1.3 Objective of Research

A layered (fiber) model is developed in order to incorporate the effects of tension stiffening and softening of concrete. The moment curvature relationships are then computed by trial and error. These are compared to the experimental results obtained by Berwanger et al. (1960). Thus the influence of the above mentioned effects on moment curvature relationships are studied. Also in some cases axial loads are included and their effects are observed.

Chapter 2 discusses the phenomenon of tension stiffening and softening of concrete and their effects. The layered (fiber) model is also explained along with the

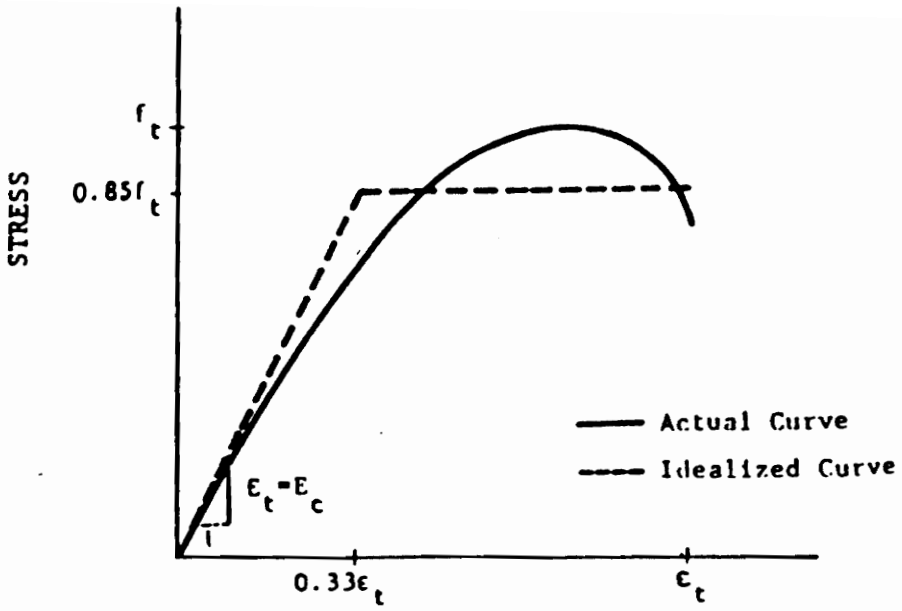

$$f_t = 1.7\ (f'_c\ \text{psi})^{2/3}\ \text{psi}$$

$$= 0.17\ (f'_c\ \text{Ksi})^{2/3}\ \text{Ksi}$$

$$\varepsilon_t = 2.571\ f_t\ /\ E_t$$

Figure 1.4. Stress-Strain Curve for Concrete in Tension adopted by El-Metwally and Chen

method employed to obtain the moment-curvature curves. Chapter 3 gives the results of the study. Discussions and conclusions are presented in Chapter 4.

Chapter 2: Effects and Methods

2.1 Tension Stiffening

A reinforced concrete flexural member, when subjected to loads, undergoes cracking in the tensile zone. However, the concrete in between the cracks tend to remain intact. The reinforcement bars help carry the tensile forces across the cracks. In between the cracks concrete is able to carry tensile stresses locally. The stresses are mainly carried in the direction of the reinforcement and can be attributed to the bond between steel and concrete. Also concrete does not undergo cracking completely and suddenly. Instead it undergoes cracking micro-progressively. This factor is another reason cracked concrete carries tensile stresses. This whole phenomenon is termed 'tension stiffening'.

2.2 Effects of Tension Stiffening

The tension stiffening effect has significant influence on the overall bending stiffnesses of a member. The effect is usually large in beams under service loading. The

curvature of reinforced concrete beams under service loading is significantly larger than that calculated on basis of uncracked sections. Curvature calculations based on cracked sections are usually smaller than actual. In a cracked reinforced concrete flexural member, the intact concrete between each pair of adjacent tensile cracks assists the tensile steel in carrying the internal tensile force and therefore contributes to the overall bending stiffnesses of the member. With increase in load secondary cracks form around the reinforcement and between the primary cracks which results in a gradual decrease in the effect.

2.3 Softening of Concrete

As strain increases in concrete, a peak stress is reached. After this peak stress is reached, the stress gradually decreases. This can be observed in both compression and tension, and the phenomena is termed 'softening' of concrete. Any realistic analysis should include this phenomenon in both post-peak tension and compression. However, it is usually omitted due to convergence problems and computational difficulties. El-Metwally and Chen (1990) have indicated that the omission of this effect in tension has led to some disparities.

2.4 Methods

Moment-curvature plots are drawn in order to compare the results to those obtained in experiments by Berwanger et al. (1960). The calculations are done on Microsoft Excel versions 3.0/4.0. A spreadsheet is selected over writing a computer program as it has some distinct advantages. Any changes made will immediately lead to

the recalculations of the related quantities. This is of a great help in a trial and error process. Once the moment and curvature values have been calculated, graphs can be obtained with little difficulty. The graphs will also reflect any relative changes made. Other spreadsheets are available, such as Quattropro and Lotus. Microsoft Excel is used in this study as some of its features are particularly helpful and are not available in the other software. For example, in Excel a cell can be assigned a symbol (such as E_c) and in all computations the cell can be referred to by E_c instead of , say A8. This avoids confusion as formulae can be written in their original form and not as a series of cell addresses. Another distinct advantage is that a graph can be attached to the spreadsheet itself, which makes it easier to see the changes immediately (see Figure 2.1).

2.5 Layered Element

To obtain the relationship between moment and curvature, the following steps are executed. The beam cross-section is divided into layers (fibers). Figure 2.2 shows a fiber model. Strain and corresponding stresses can be obtained at these layers and hence lead to more accurate calculations. The layers are selected at an interval between 0.25 inches and 1 inch. The interval chosen is governed by the depth of the beam and the number of calculations involved. In most cases this is chosen as 0.25 inches. These layers are also chosen such that there will be a fiber at the level of both tensile and compression steel (if present). Strain is assumed to vary linearly across the cross-section. The moment-curvature values are obtained by trial and error. First a curvature 'ψ' is selected and the strain at the extreme layer and at the level of tensile steel is calculated. To do this a trial value of the location of the neutral axis is assumed. Strains at various levels are then filled in using interpolation. The next step is to adjust the location of the neutral axis until the

BEAM C1		Idealized tension curve	
Curvature 'Psi" =		2.00E-04	
Eff. Dept. d =		5.5	
Dept to NA c = kd =		1.8957	
		Fiber 1	Fiber 2
Level		0	0.25
Strain		0.00037914	0.00032914
Stress		1398.700254	1303.212339
Total Force		547.2414743	1019.763655
Moment about T		2941.422924	5226.288732
Total Compressive Force C =			4599.058785
Total Tensile Force T =			-4599.0868
Moment =			23007.30394

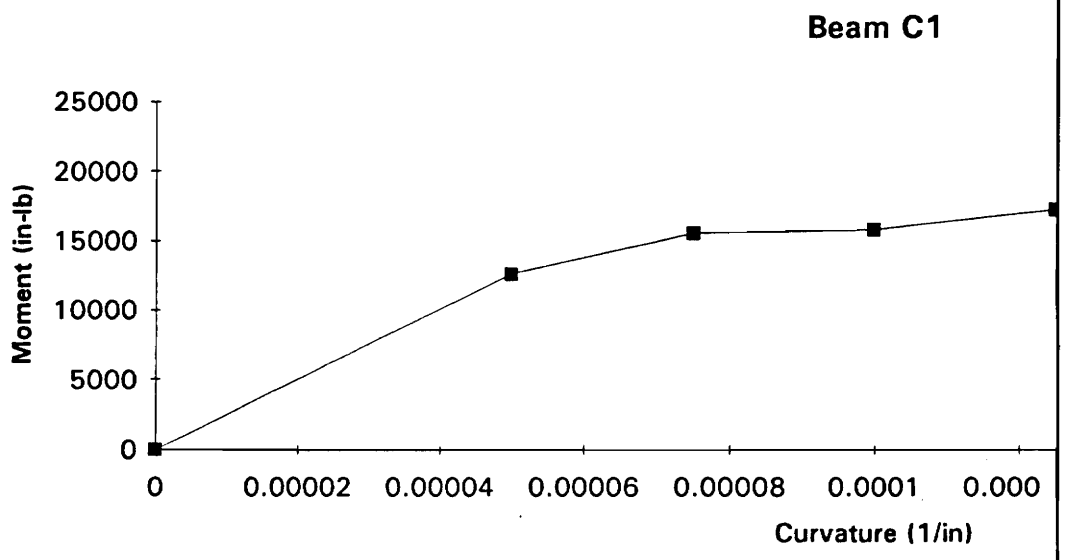

Figure 2.1 Printout from Excel

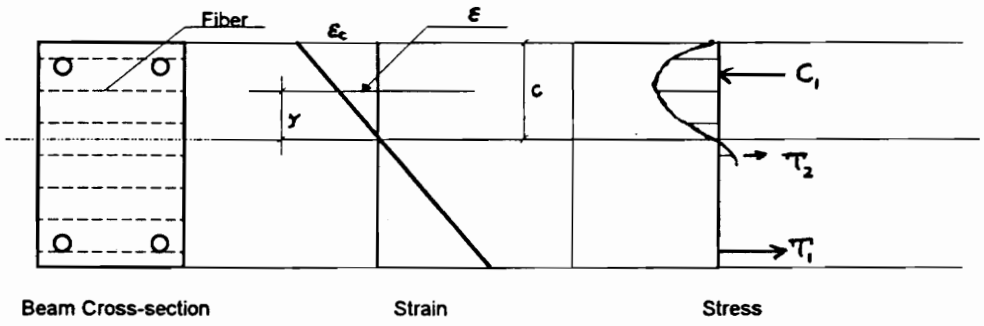

$$\psi = \frac{\varepsilon_c}{c}$$

Figure 2.2 Layered (fiber) Element

forces are balanced. This procedure is explained in the next paragraph.

Stress-strain diagrams used by El-Metwally and Chen have been adopted here. Descriptions of these stress-strain diagrams are given in Chapter 1. The stress-strain curve in compression depends on the effective depth of the cross-section. Thus the stress varies with change in the effective depth. Both tensile and compressive stress-strain curves are plotted in one part of the spreadsheet. The compressive stress-strain curve is computed making use of the value of effective depth entered. Hence any changes made will be incorporated in the curve (Figure 2.3). For strains at each level, corresponding stresses are obtained from the stress-strain curves already drawn. In the tensile zone, tensile strains beyond ε_t are assumed to have zero stress, i.e., neglected. The compressive and tensile forces are then calculated by integrating the stresses over their corresponding areas, i.e., by multiplying with the width and depth of the layer. Now by trial and error the depth of the neutral axis is varied until the total compressive force 'C' equals the total tensile force 'T' (Figure 2.1). Now the moment of this couple is calculated by multiplying by the distance between the two forces. The moment and curvatures are then noted down. This procedure is repeated for different values of curvatures to obtain corresponding moments. The plot of moment versus curvature is then drawn.

2.6 Inclusion of Tension Stiffening and Softening of Concrete

The stress-strain curve adopted by El-Metwally and Chen for concrete in compression does include the softening behavior of concrete in compression. However, the tensile curve adopted by these authors does not include the behavior. In this study the behavior is included for tensile curves also. This is achieved by adopting a realistic stress-

BEAM C1		
STRESS- STRAIN CALCULATION		
Width of Cross-Section	w	3.13
Depth of Cross-Section	d	5.5
Depth of Neutral Axis c = kd	kd	2
Cross- Sectional area of transverse reinforcement	Astr	0.11
Area of concrete under compression	Ac	6.26
Area of bound concrete under compression	Ab	1.13
Breadth of bound concrete cross-section	ww	1.13
Effective depth of bound concrete cross-section	dd	4.5
longitudinal spacing of transverse reinforcement	S	8
Compressive strength of concrete	fc	3000
Longitudianal Spacing at which tra. reinf. ineffective	So	10
	B	4.5
	q	-0.02574
	Ec = Et	3.44E+06
	ece	0.001744
	ecs	0.002436
	ecf	0.004402
	ft	353.6142
	et	0.000264

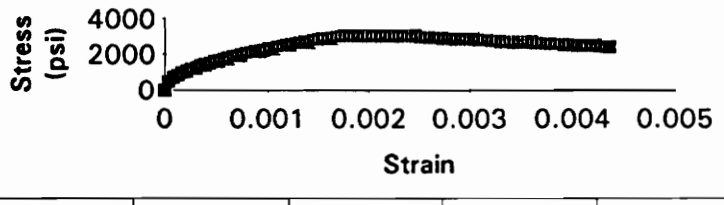

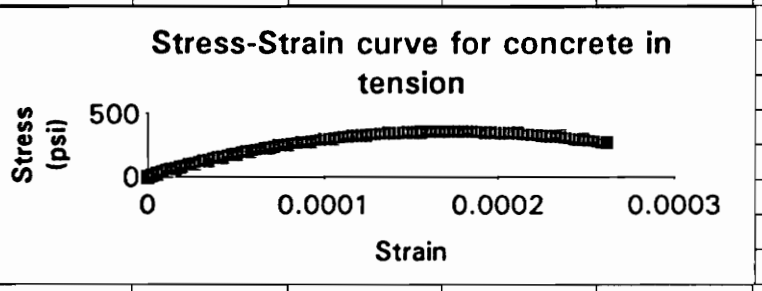

Figure 2.3 Stress-strain diagram on Excel along with calculations

stain curve in both tension and compression. Moment-curvature curves are calculated using the improved idealized stress-strain curve for concrete. These are discussed further in Chapter 3.

When the stresses at each layer are calculated, tensile stresses are also included. Thus the tension stiffening effect is included in the method. However stresses resulting from strains greater than ε_t are neglected. This is employed due to the formation of secondary cracks which reduces the tensile carrying ability of concrete.

2.7 Inclusion of Axial Load

By calculating the moment, after setting C = T, no axial load is assumed to act on the cross-section. To include the effect of axial load the following is done. Moment curvature curves are drawn for cross-sections with axial loads expressed as a fraction of P_u, where P_u is the ultimate load carrying capacity of the cross-section. Curves are drawn for $0.1P_u$, $0.2P_u$, $0.3\ P_u$, $0.4P_u$, $0.5P_u$ and $0.9P_u$. To do this the difference between the compressive force C and tensile force T is set equal to the magnitude of the axial load, with C greater than T. Moment is then calculated as usual.

Chapter 3: Results

3.1 Experimental work by Berwanger et al. (1960)

Berwanger et al. have tested series of beams and given the moment-curvature relationships for different beams at various sections. The experimental setup consists of two series. The first series consists of two beams labeled C1 and C2. These are simply supported, singly reinforced beams. The beams have a single span equal to 48". The width and effective depth are 3.13" and 5.5" respectively. The tensile reinforcement consists of two #3 bars. Both beams are subjected to two concentrated loads at L/3 from each support, where L is the span of the beam. Beam C1 has a stirrup spacing of 4" whereas beam C2 has a stirrup spacing of 2". Beam C1 is chosen from this group for our study.

The second set of beams consisted of six two-span beams with varying properties. Here studies are conducted on Beam 5. The two equal spans measure 48". This beam is subjected to two concentrated loads at L/2 in each span. The beam has a breadth and

effective depth of 3.13" and 5.5" respectively as in the case of the first series. The other details of the beam are as in Figure 3.1. The figure also shows the reinforcement details.

3.2 Variation in Stress-Strain Curve

The maximum compressive stress f_c' is governed by a factor 'q' in El-Metwally and Chen's stress-strain curves for concrete in compression. They are given by:

$$f_c' = 0.9U_{cyl}(1+0.05q) \qquad \text{.....(3.1)}$$

$$q = \left(1.4\frac{A_b}{A_c} - 0.45\right)\frac{A_{st}(S_0 - S)}{A_{st}S + 0.0028BS^2} \geq 0 \qquad \text{.....(3.2)}$$

where A_{st} = Cross-section area of transverse reinforcement

A_c = Area of concrete under compression

A_b = Area of bound concrete

b_1 = Breadth of bound concrete

d_1 = Effective depth of bound concrete cross-section

B = b_1 or $0.7d_1$ whichever greater

S = Longitudinal spacing of transverse reinforcement $\leq S_0$

S_0 = Longitudinal spacing at which transverse reinforcement is not effective (taken as 10")

U_{cyl} = Standard 6"x12" cylinder compressive strength.

This factor q in turn depends on the above listed factors. El-Metwally and Chen have made an attempt to include the effects of these factors. When the spacing of the

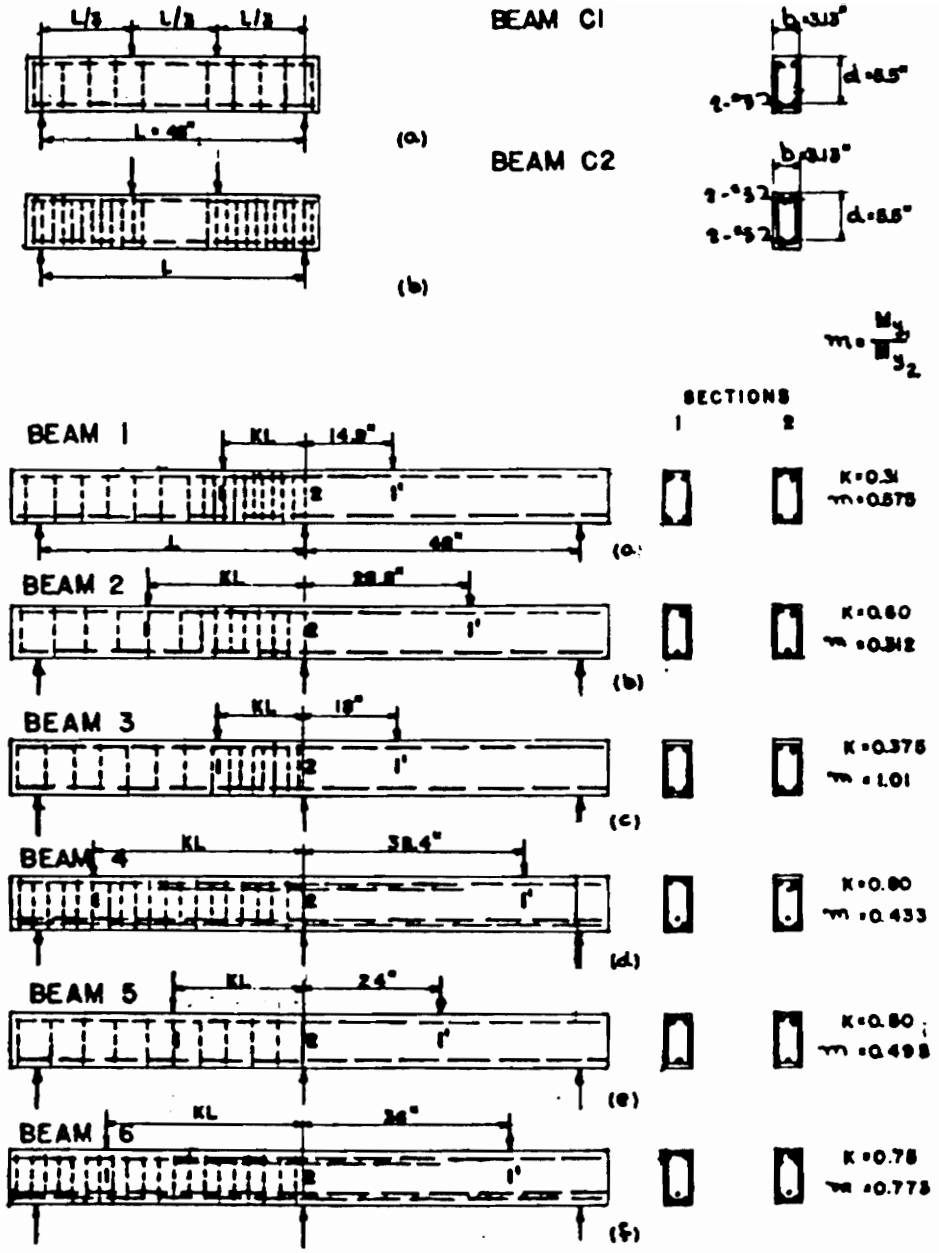

Figure 3.1 Details of Beams tested by Berwanger et al. (1960)

transverse steel 'S' is equal to 10", i.e., equal to S_0, q turns out to be zero and hence has no effect on the stress. Also q is equal to zero when the area of transverse steel A_{st} is zero (when absent). The area of bound concrete A_b and the area of concrete under compression A_c, too have some effect on the curve. They have no effect when A_c is approximately three times A_b. Figure 3.2 shows El-Metwally and Chen's stress-strain curves for concrete under compression for different areas of transverse steel. Series 1 represents curves drawn assuming #2 bars, series 2, #3 bars and series 3, #4 bars. The curves are identical up to the peak stress f_c'. The softening part of the curve is not identical in all three curves. The difference seems to be small. However, it might be significant in the case of large beams and columns. Figure 3.3 shows the stress-strain curves for concrete under compression for different spacings of transverse steel. Series 1 represents curve drawn with S equal to 2.5". Series 2,3 and 4 are drawn with S equal to 5.0", 7.5" and 10.0" respectively. These curves also show no disparities up to the maximum stress f_c' (parabolic part). Once again the softening branches have slight variations, but these variations are greater than the previous case.

3.3 Beam C1

C1 is the first beam in the first series tested by Berwanger et al. (1960). This beam is chosen for this study from the series. It is a simply supported member, with a span of 48". The width and effective depth are 3.13" and 5.5" respectively, the overall depth being 6.5". The reinforcement consists of two #3 bars. Transverse steel is provided at a spacing of 4" up to 16" from either support (one third of the span). Both concrete and steel used in these beams were tested by Berwanger, et al. (1960). The maximum stress f_c' for concrete in beam C1 is 3000 psi at 7 days and 3560 psi on the day of the test. E_c is

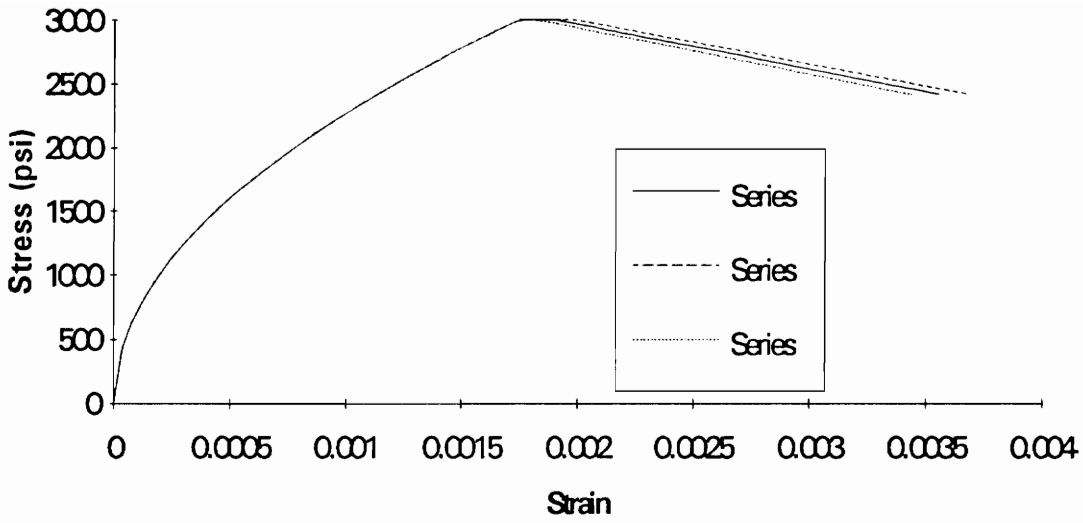

Figure 3.2 Stress-Strain curves for varying area of transverse steel

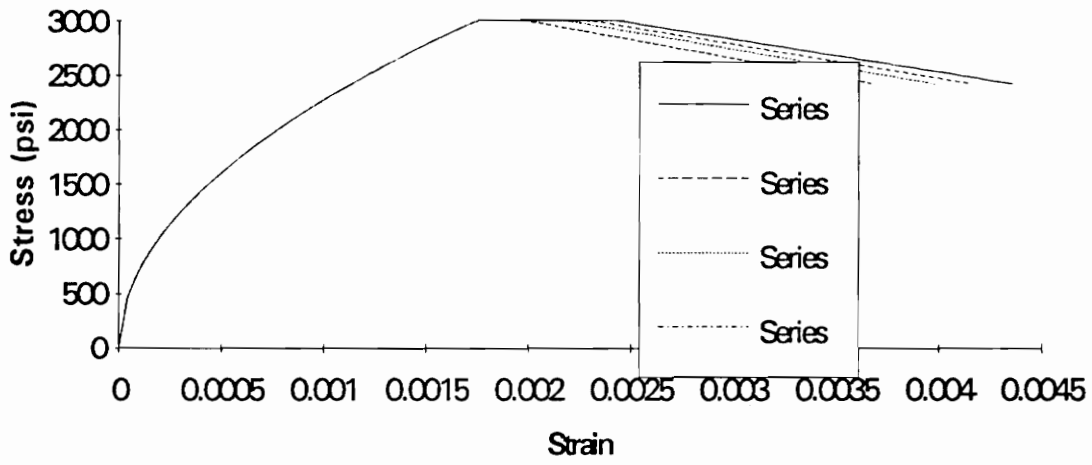

Figure 3.3 Stress-Strain curves for varying spacing of transverse steel

calculated to be 3.44×10^6 psi. Tension tests of reinforcement have indicated f_y as 44.6 ksi and E_s as 26.4×10^6 psi. The cross sectional area of the high-bond bars is measured to be 0.114 sq. in. The beam is subjected to two concentrated loads at L/3 from each support, where L is the span of the beam.

The moment-curvature relations obtained for beam C1 are presented in Figures 3.4 to 3.7. Figure 3.4 shows the curve which is drawn using the El-Metwally and Chen tensile (i.e., idealized). The graph was drawn for different ψ values starting from 0.5×10^{-4}/in. to 2×10^{-4}/in. at an interval of 0.25×10^{-4}/in. This curve does not show smooth change at curvatures below 1.0×10^{-4}/in. Moment -curvature curve using a realistic tensile curve is also drawn (Figure 3.5). This curve also does not show a gradual change in the above mentioned range. When the tensile curve is omitted (neglect tension in concrete completely), the curve smoothes out. This is shown in Figure 3.6. All three curves are shown for comparison in Figure 3.7.

3.3 Beam 5

The fifth beam in the second series of Berwanger is chosen for this study. The beam has the same cross-sectional properties as the earlier one (Beam C1). The width, effective depth and overall depth of the beam are 3.13", 5.5" and 6.5" respectively. The beam is reinforced with three #3 bars, two in the top and one at the bottom. Transverse reinforcement is provided in the form of #2 bars at 4.8" c/c. The beam is a two-span continuous beam resting on simple supports at either end. The spans are equal and measure 48". Both spans are subjected to concentrated loads at midspan. Maximum compressive stress f_c' for concrete in this beam is 1980 psi at 7 days and 2800 psi on the day of the test. E_c is calculated to be 3.35×10^6 psi. As in the case of beam C1, f_y of

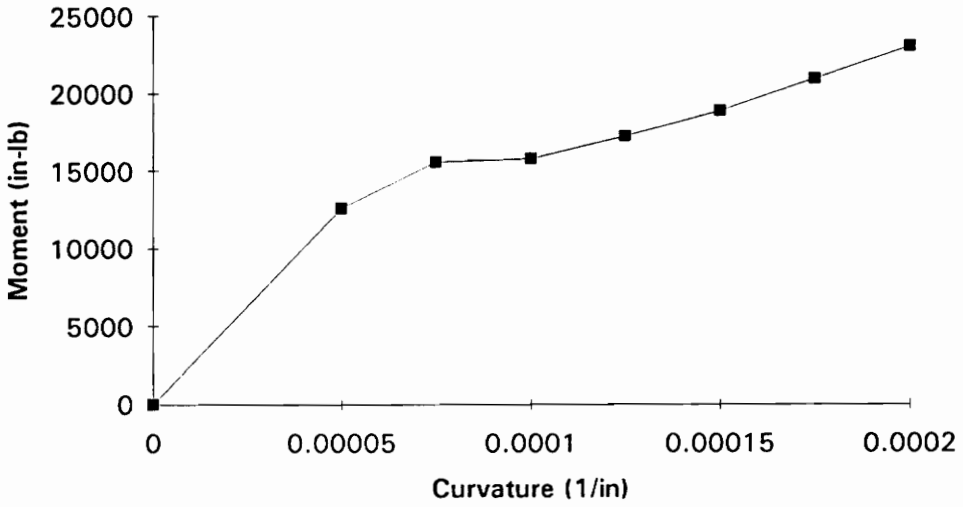

Figure 3.4 Moment-curvature curve for beam C1 with idealized tension curve

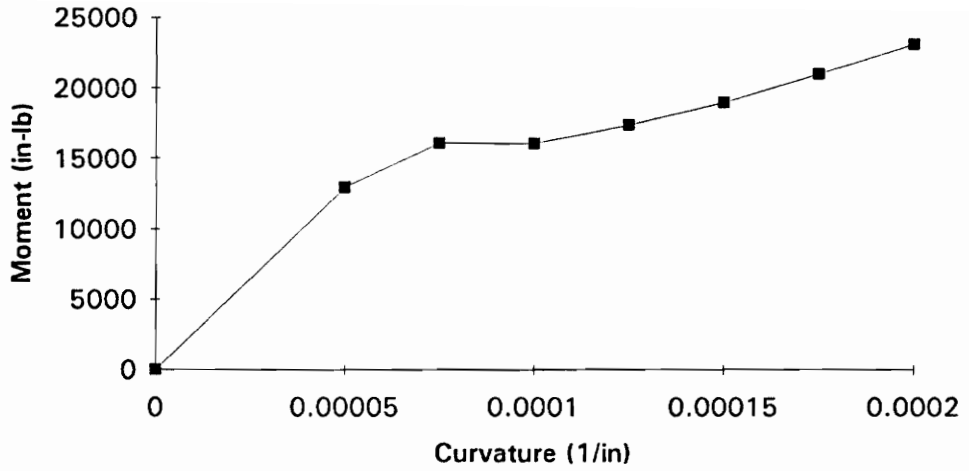

Figure 3.5 Moment-curvature curve for beam C1 with realistic tension curve

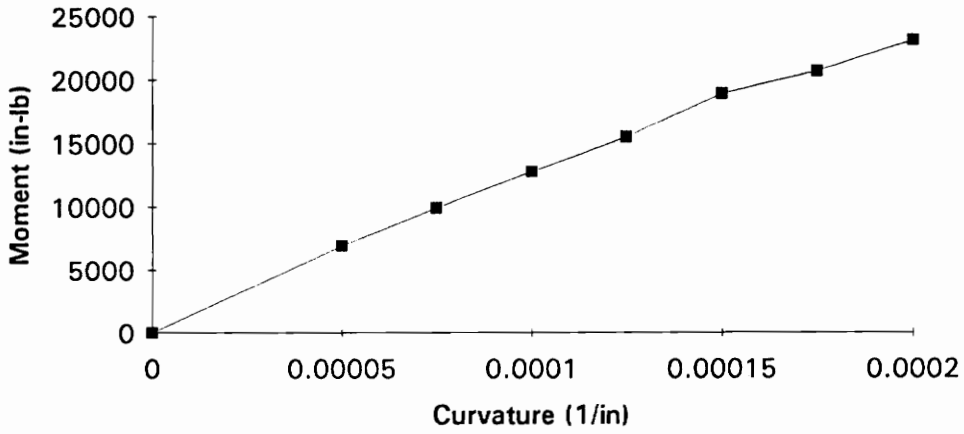

Figure 3.6 Moment-curvature curve for beam C1 with no tensile curve

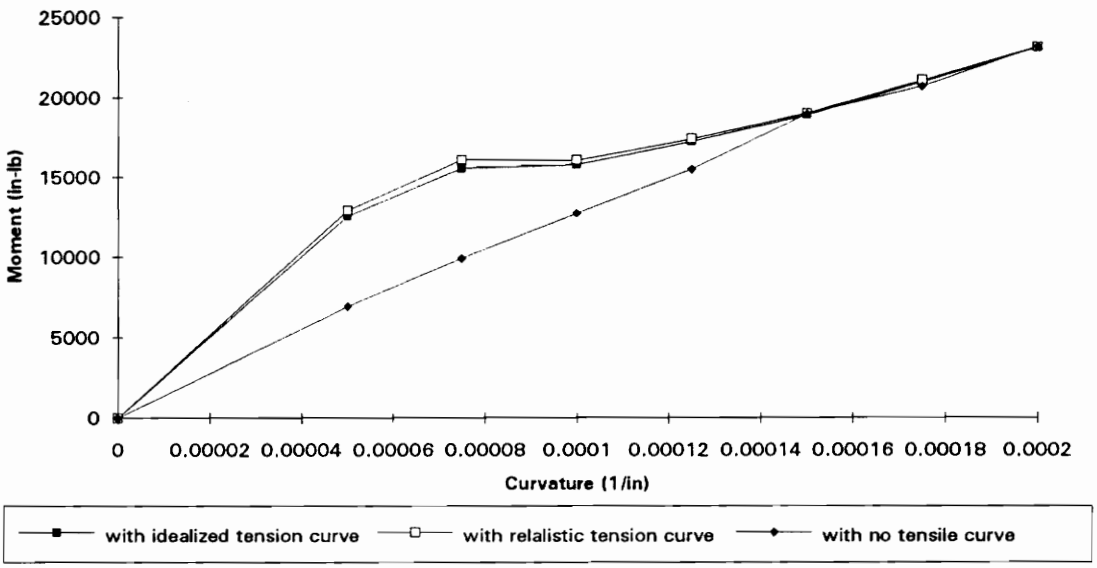

Figure 3.7 Moment-curvature curve for beam C1 with all three curves

steel is 44.6 ksi, Es equals 26.4 $\times 10^6$ psi and cross-sectional area 0.114 sq. in. Further details can be obtained from Figure 3.1.

Berwanger, et al. (1960) has given moment-curvature relations for this beam at two different sections. Studies are done for both sections and are referred to as Section 1 and Section 2. Figure 3.8 shows the moment-curvature curve for Beam 5 Section 1. This relationship has been obtained using the El-Metwally and Chen stress-strain curves (realistic). The next graph (Figure 3.9) shows M-ψ relationships for the same section, obtained by omitting the tensile curve. The two graphs have been shown together for comparison in Figure 3.10. The abrupt changes in the M-ψ curve vanish in the second case, i.e., when no tensile curve is used as in the case of Beam C1. The experimental results of Berwanger are in Figure 3.11. The two curves obtained analytically can also be seen in the graph. The graph drawn with El-Metwally and Chen curves without tension is more in agreement than the one with tension.

3.4 Beam-Column

Apart from the beams tested by Berwanger, the same method was employed to study a beam-column. The dimensions of the beam-column are taken as 16" $\times$ 20". It is reinforced with 8 bars symmetrically placed. Ties are provided in the form of #3 bars at 6" c/c. Concrete compressive stress f_c' is assumed as 3000 psi and f_y of steel 60 ksi. Figure 3.12 shows the M-ψ curves for this beam-column with no axial load. Here three different M-ψ curves are drawn by changing the cross-sectional area of the reinforcement used. M-ψ curves have been obtained for #6, #8 and #11 bars.

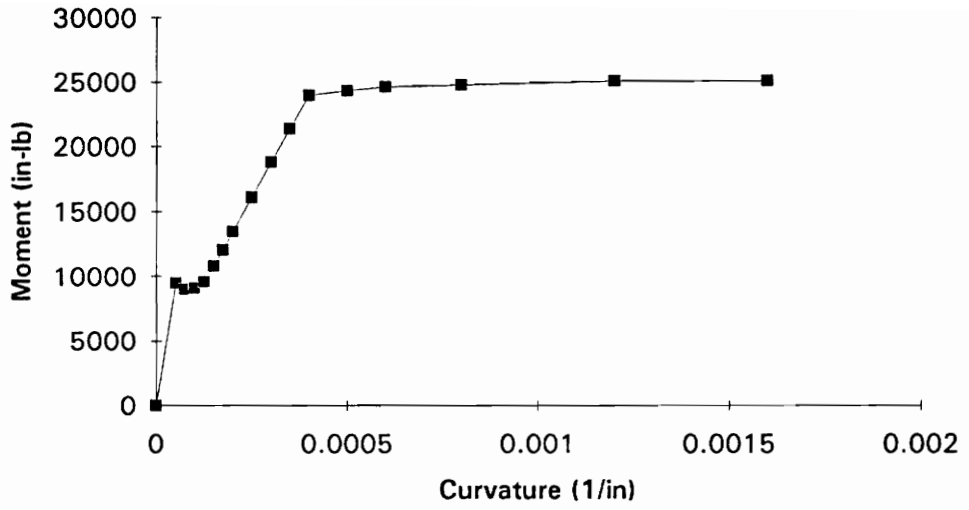

Figure 3.8 Moment-curvature curve for beam 5 (El-Metwally and Chen curves with tension)

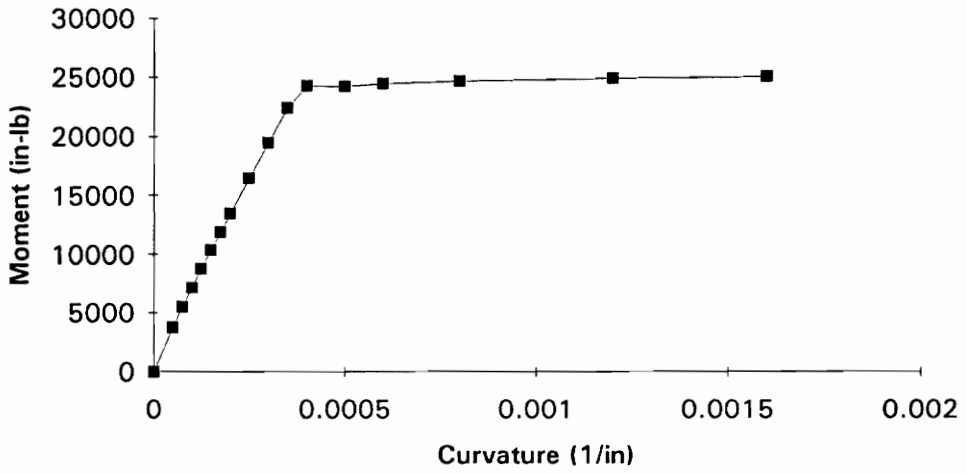

Figure 3.9 Moment-curvature curve for beam 5 (El-Metwally and Chen curves without tension)

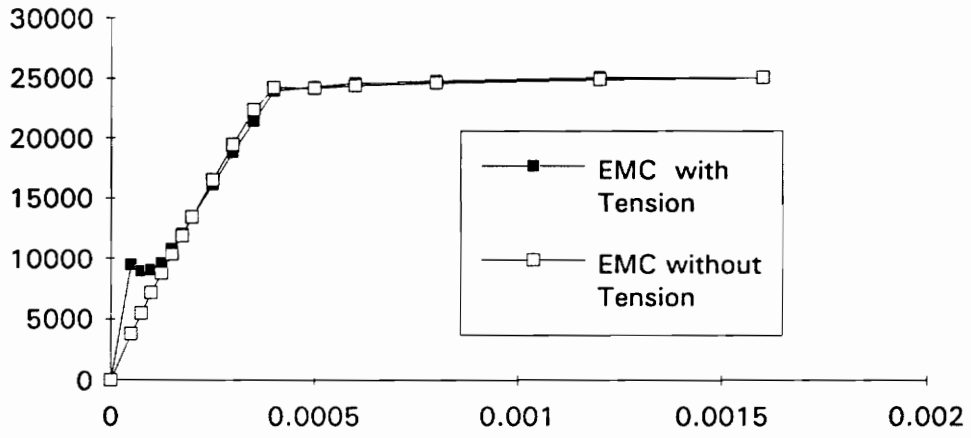

Figure 3.10 Moment-curvature curve for beam 5 with and without tension

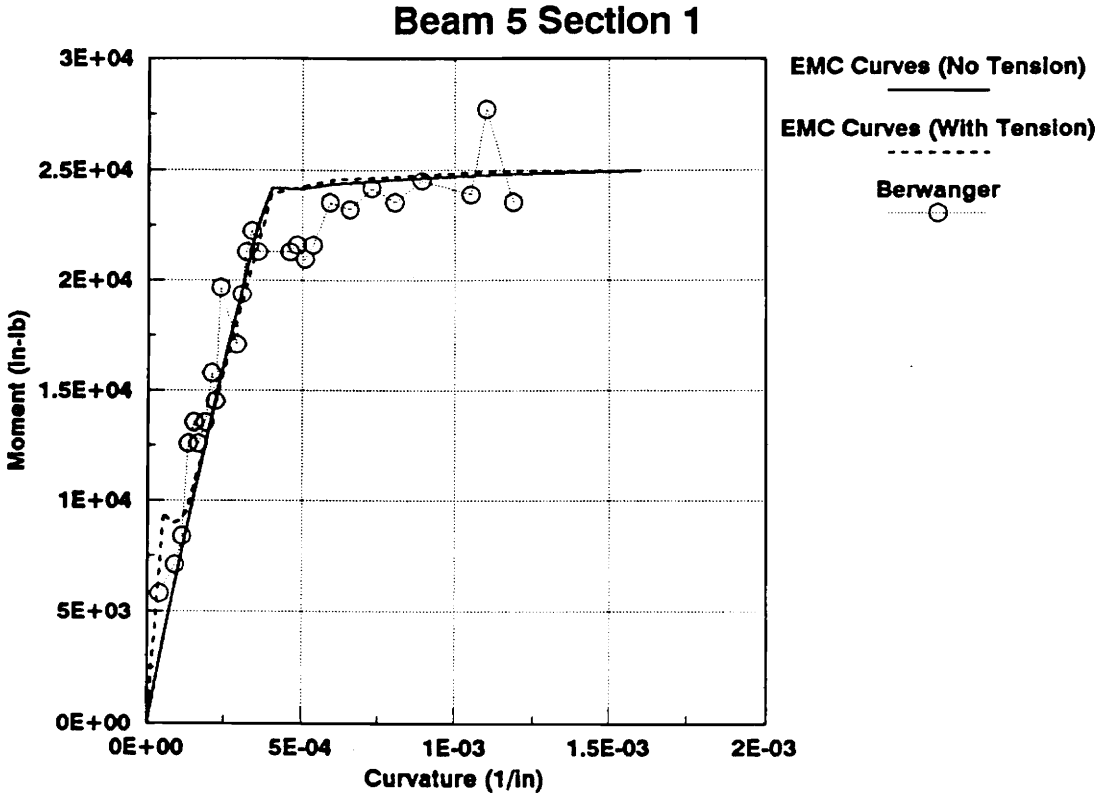

Figure 3.11 Experimental results obtained by Berwanger along with analytical results

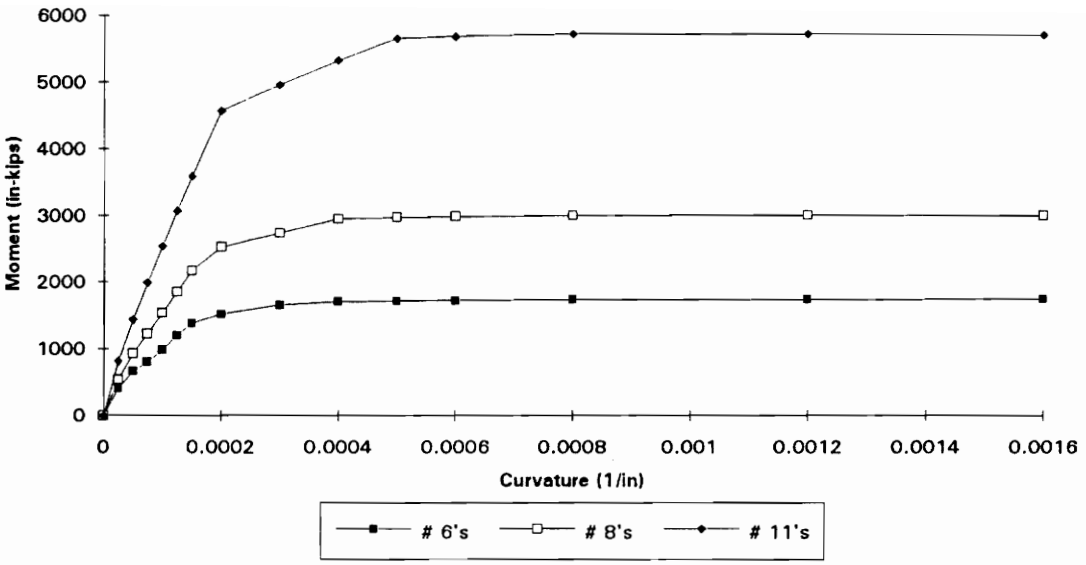

Figure 3.12 Moment-curvature for Beam-Column without Axial Load

3.5 Effect of Axial Load

As explained in Chapter 2, axial load is introduced to study its effects. Moment-curvature relationships are obtained after introducing axial load as a percentage of P_u, where P_u is the ultimate load carrying capacity of the cross-section. Figure 3.13 shows the M-ψ curves for the beam-column mentioned above, for different reinforcement percentages with an axial load of 0.2 P_u. Comparing with Figure 3.12, it can be seen that the moment carrying capacity of the cross-section has increased with the introduction of the axial load. This is true for all three cases, i.e., with #6, #8 and #11 reinforcement bars. Further to see its effects at larger percentages of Pu, M-ψ relationships are obtained for different magnitudes of the axial load, leaving the reinforcement percentage constant, i.e., using #8 bars. This is shown in Figure 3.14. The axial load is increased from $0P_u$ to $0.5P_u$, with an increment of $0.1P_u$. The moment carrying capacity of the section increases steadily with increase in axial load. This increase occurs until the axial load reaches 0.6 to 0.7 Pu, after which any increase in Pu decreases the moment carrying capacity. When the axial load is in the range of 0.5 to 0.7 Pu, the increased moment capacity does not sustain. It tends to decrease suddenly with increase in curvature. Figure 3.15 shows M-ψ curves for different axial loads for Beam 5 Section 1. Here too, this trend can be observed.

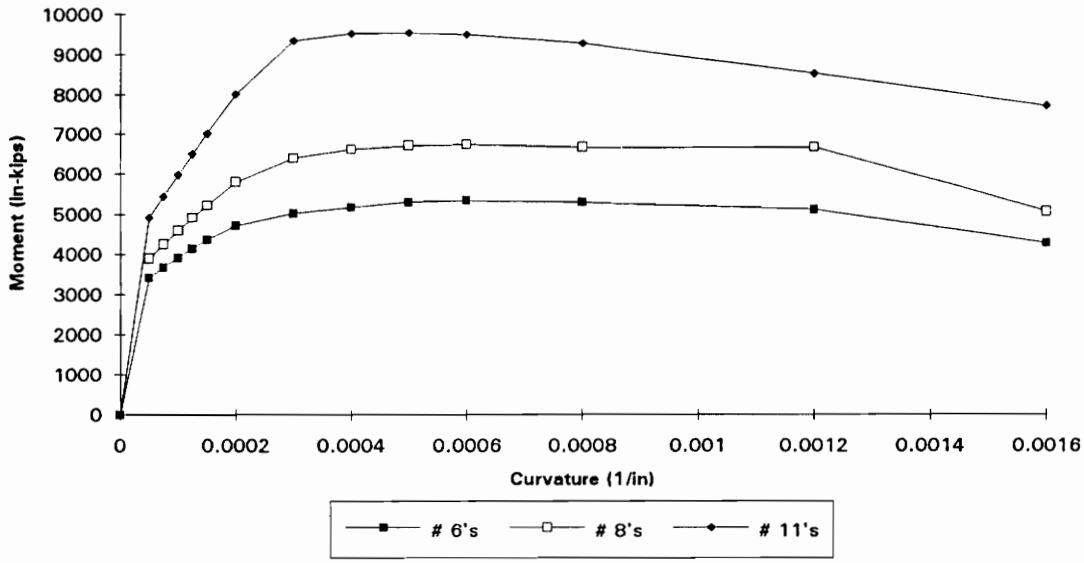

Figure 3.13 Moment-curvature for Beam-Column with 0.2 Pu

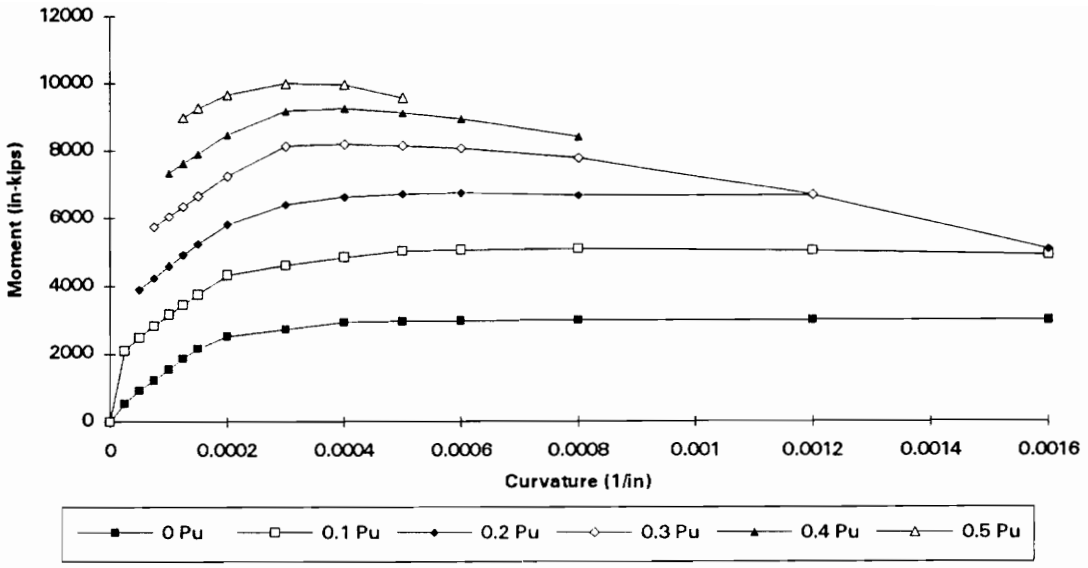

Figure 3.14 Moment-curvature for Beam-Column 8 #8's with varying Pu

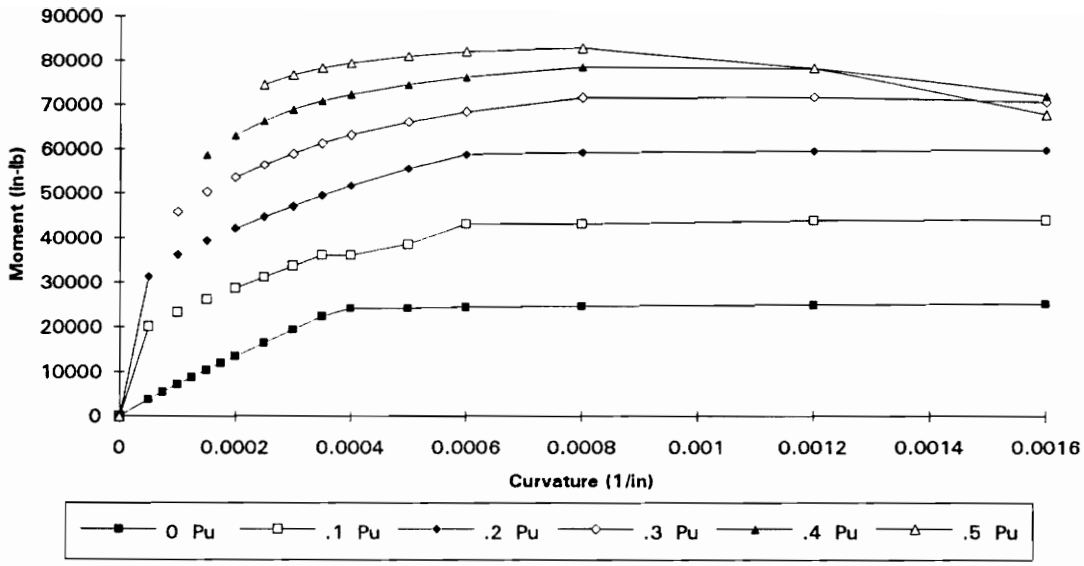

Figure 3.15 Moment-curvature for Beam-5 Section 1with varying Pu

Chapter 4: Discussions and Conclusions

4.1 Fiber Model: Advantages and Disadvantages

The fiber (layered) model offers some distinct advantages and disadvantages. The first and foremost advantage is accuracy. Since the model is divided into many layers and stresses and strains are obtained at many points the behavior is better predicted and the moment and curvature calculations are more accurate. Especially in the concrete tensile zone, since even the smallest stress is taken into account, the model gives better results. The second advantage is the simplicity of the model.

On the negative side, the calculation involves the assumption of depth of NA for calculation of the forces. By trial and error these forces are equated to find the actual NA.

Moment and Curvature values are calculated at this point. This sometimes is cumbersome and takes a lot of computation time.

4.2 Tension Stiffening and Softening

As explained in Chapter 2, the effect of tension stiffening is included. This was achieved by introducing tensile stresses in the tensile zone of concrete at different layers of the model and including them in the computation of the axial forces. Softening of concrete is introduced by adopting a realistic stress-strain behavior of concrete in both compression and tension. The disparities between the analytical results obtained by El-Metwally and Chen and the experimental data of Berwanger et al. is given in Chapter 1. According to El-Metwally and Chen, the disparities are possibly due to the tension stiffening and softening of concrete. The results of this study are presented in Chapter 3. The moment-curvature relationships obtained by using El-Metwally and Chen's stress-strain curve (including the softening effect) are in agreement with the experimental results of Berwanger. However the analytical results show an abrupt change in stiffness immediately after cracking. This change vanishes when the analytical results are calculated after omitting the tensile curve.

4.3 Axial Load

The strength of the section increases proportionally with increase in axial load. This occurs usually in the range of 0.6 to 0.7 Pu. This increased moment capacity does not sustain. It tends to decrease with increase in curvature. At high axial loads the

moment capacity decreases. The ductility however, decreases with increasing axial compression. This behavior is well known and observed.

4.4 Further Study

This study involves the development of the fiber model and studying moment-curvature relationships by calculating them using realistic stress-strain curves. The study can be further extended by including torsional effects on the beam. Also shear deformation can be included in the study.

By using the effect of tension stiffening and the softening of concrete in non-linear analysis of reinforced concrete structures, the prediction of the structural behavior is expected to be better. This can be done, for example, by defining user-defined stress-strain curves. This was attempted on 'ABAQUS', the finite element analysis software. Due to the complexity of the problem and the time constraints, this was not completed.

4.5 Conclusions

The moment-curvature curves do not show a large deviation from El-Metwally and Chen's results when realistic tensile stress-strain curves are used. The curves tend to smoothen out when the curves are drawn with no tensile curves at all. This can be observed both in the case of Beam C1 and Beam 5. Both the beams, however, follow the observed tendencies when subjected to an increase in axial load, i.e., when they behave like beam-columns. The last 16 × 20 beam-column also follows a similar trend.

References

1. Alwis, A.M., "Trilinear Moment-Curvature Relationship for Reinforced Concrete Beams," ACI Structural Journal, V 87 No 3, May-June 1990, pp 276-283.

2. Bazant, Zdenek P., Pijaudier-Cabot, Gilles, and pan, Jiaying, "Ductility, Snapback, Size Effect, and Redistribution in Softening Beams or Frames", Journal of the Structural Division, Vol 113, No. 12, December, 1987, pp 2348-2364.

3. Berwanger, C.; Marshall, W.T.; Siev, A.; and author, Discussion of "Comparison of Measured and Calculated Stiffnesses for Beams Reinforced in Tension Only" by Bill G. Eppes, ACI Journal, Proceedings V. 56, No 12, June 1960, pp 1345-1356.

4. Cosenza, Eldorado, Greco, Carlo, and Pecce, Marisa, "Nonlinear Design of Reinforced Concrete Continuous Beams", Science and Technology, January 1991, pp 19-27.

5. Desai, C.S., "Elementary Finite Element Method", 1979, Prentice-Hall Inc.

6. El-Metwally, Salah E., and Chen, Wai-Feh, "Load-Deformation Relations for Reinforced Concrete Sections", ACI Structural Journal, V 86, No 2, March-April 1989, pp 163-167.

7. Gajer, Grzegorz, and Dux, Peter F., "Strain-Softening Analysis of Concrete Structures", Computers and Structures, Vol 33, No. 2., 1989, pp 575-582

8. Gilbert, R. Ian, and Warner, Robert F., "Tension Stiffening in Reinforced Concrete Slabs", Journal of the Structural Division, December 1978, pp 1885-1900.

9. Holzer, Siegfried M., Somers, Arnold E Jr., and Bradshaw, Joel C., "Finite Response of Inelastic RC Structures", Journal of the Structural Division, Proceedings of the ASCE, January 1979, pp 17-33.

10. Hu, Hsuan-Teh., and Schnobrich, William C., "Non-linear Analysis of Cracked Reinforced Concrete", ACI Structural Journal, V 87, No 2, March-April 1990, pp 199-207.

Vita

M.N. Nagendra Prasad was born in Mysore, India in May 1968. He obtained his Bachelor of Engineering degree from Mysore University, India in October 1989. He worked in India for an year in the capacity of a Design Engineer, before starting higher studies here at Virginia Tech from January 1991. He plans to pursue a career back home after his graduation.